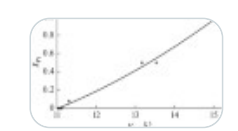


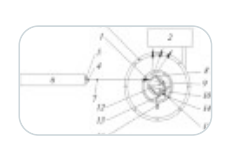
31 articles in this issue

Features of Nanostructured M_x -Pt_{1-x} (M = Fe, Co, Ni) Solid Solutions Obtained by Precursor Reduction in Aqueous Solutions



OriginalPaper | 25 September 2025 | Pages: 545 - 552

Application of the Method of Dynamic Diffractometry Using Synchrotron Radiation to Study Phase Formation Processes during the Synthesis of a Mechanically Activated Ti–Al–C Mixture



OriginalPaper | 25 September 2025 | Pages: 553 - 561

Maximum Achievable Diffraction Efficiency of Neutron Low-Frequency Gratings with Different Groove Profiles



OriginalPaper | 25 September 2025 | Pages: 562 - 567

Rotating Water-Jet-Cooled Target for Compact Neutron Source



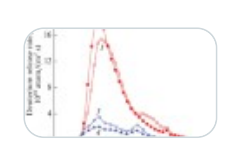
OriginalPaper | 25 September 2025 | Pages: 568 - 573

$\frac{\text{Changes in the Structure and Properties of Fluorocarbon Coatings under Irradiation with}{\text{Accelerated C}_{60} \text{ lons}}$



OriginalPaper | 25 September 2025 | Pages: 574 - 581

<u>Dynamics of Deuterium Release from EK-181 and Eurofer Steels Depending on Storage</u> Conditions



OriginalPaper | 25 September 2025 | Pages: 582 - 589

Characterization of Parent Austenite of Martensitic and Bainitic Steels Based on Their Texture Developed during Phase Transformation



On Clustering in Real Cottrell Nanosegregations in Metallic Materials



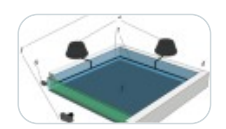
OriginalPaper | 25 September 2025 | Pages: 598 - 604

Regularities of Crystallographic Texture Formation in Austenitic Steel during Rolling and Tensile Testing



OriginalPaper | 25 September 2025 | Pages: 605 - 615

Experimental Observation of Transition from Two-Dimensional Turbulent Vortex Flow of Water to Three-Dimensional



OriginalPaper | 25 September 2025 | Pages: 616 - 620

Properties of Interface Structures Based on Oxidized Lead Selenide



OriginalPaper | 25 September 2025 | Pages: 621 - 626

On Determination of Diffusion Coefficient of an Inclusion Attached to a Fixed Dislocation Using Its Thermal Motion



OriginalPaper | 25 September 2025 | Pages: 627 - 632

Structural Transformations in Bimetallic Ni-Ag Nanoparticles with a Janus Structure



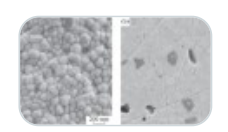
OriginalPaper | 25 September 2025 | Pages: 633 - 639

Features of the Morphology and Composition of Stones in the Human Body in the Study of the Mechanisms of Their Formation



OriginalPaper | 25 September 2025 | Pages: 640 - 646

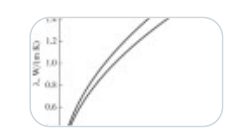
Wear Resistance and Surface Roughness of ATZ Ceramics with Different Silica Contents



OriginalPaper | 25 September 2025 | Pages: 647 - 652

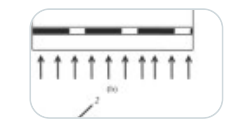


Synthesis of Fullerenes C₆₀ and C₇₀



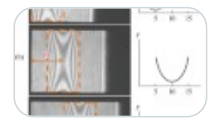
OriginalPaper | 25 September 2025 | Pages: 658 - 664

Layered-Fiber Composite with a Niobium-Based Matrix Reinforced with Carbon Fibers



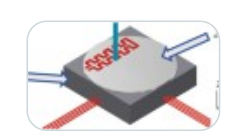
OriginalPaper | 25 September 2025 | Pages: 665 - 669

Interference Techniques for Measuring the Surface Profile of Extended Samples



OriginalPaper | 25 September 2025 | Pages: 670 - 675

Control of the Plate Movement in Extreme Ultraviolet Scanners Based on Optimal Performance Algorithms



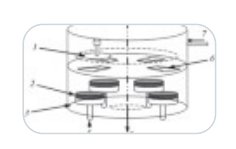
OriginalPaper | 25 September 2025 | Pages: 676 - 683

Influence of Solar Cosmic Rays on the Photometric Characteristics of the CCD Detector of the Lasco/C3 Space Telescope



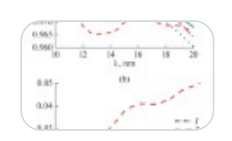
OriginalPaper | 25 September 2025 | Pages: 684 - 691

Study of the Effect of Carbon Barrier Layers on the Structural and Reflective Properties of Multilayer X-ray Mirrors Based on the Cr/V Material Pair



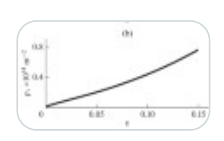
OriginalPaper | 25 September 2025 | Pages: 692 - 696

Upgraded Rubidium-Based Multilayer Mirrors for Operation in the Radiation Wavelength Range of 11.4–17 nm

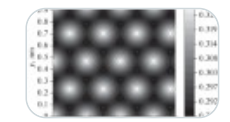


OriginalPaper | 25 September 2025 | Pages: 697 - 702

<u>Deformation</u>, Fracture, and Structure of a Single-Crystal Intermetallic Compound in Multilevel Model of Plastic Deformation



Monte Carlo Modeling of the Graphene Moiré Structure on an Ir(111) Substrate



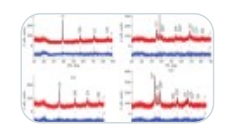
OriginalPaper | 25 September 2025 | Pages: 710 - 716

New Hybrid Multicomponent Selenium-Containing Nanosystems for Photodynamic Therapy



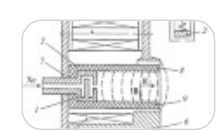
OriginalPaper | 25 September 2025 | Pages: 717 - 728

Hydride Phases Based on High-Entropy Alloys TiZrTaV($Mo_{1-x}Nb_x$) and TiZrTaNb($Mo_{1-x}Ni_x$), x = 0.2, 0.4, 0.6, and 0.8



OriginalPaper | 25 September 2025 | Pages: 729 - 738

Study of the Possibility of Increasing the Thrust Efficiency and Service Life of Stationary Plasma Thrusters Operating on Krypton



OriginalPaper | 25 September 2025 | Pages: 739 - 753

Study of the Integral Characteristics of a Radio-Frequency Ion Thruster Operating on Krypton and Estimation of the Service Life of Its Ion-Extraction System



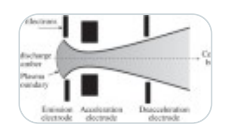
OriginalPaper | 25 September 2025 | Pages: 754 - 763

Peculiarities of Determination of Self Electromagnetic Emission from Pulsed Plasma Thrusters



OriginalPaper | 25 September 2025 | Pages: 764 - 770

Modeling the Process of Deposition of Erosion Products on the Walls of the Gas-Discharge Chamber of an Ion Thruster



OriginalPaper | 25 September 2025 | Pages: 771 - 782